Simulation of Deformation and Aggregation of Two Red Blood Cells in a Stenosed Microvessel by Dissipative Particle Dynamics

L.L. Xiao[1, 2], Y. Liu*[1], S. Chen[2] and B.M. Fu[3]

[1]Department of Mechanical Engineering, The Hong Kong Polytechnic University, Hong Kong, China

[2]School of Aerospace Engineering and Applied Mechanics, Tongji University, Shanghai, China

[3]Department of Biomedical Engineering, The City College of the City University of New York,
New York, NY, USA

*Corresponding author: yang.liu@polyu.edu.hk

Abstract

The motion of two red blood cells (RBCs) in a stenosed microvessel was simulated using Dissipative Particle Dynamics. The effects of intercellular interaction, RBC deformability and the initial cell orientation on the deformation and aggregation of the RBCs and on the flow resistance were investigated. The RBC membrane was treated as a three-dimensional coarse-grained network model and the intercellular interaction was modeled by the Morse potential based on a depletion-mediated assumption. It is shown that the flow resistance increases dramatically when the RBCs enter into the stenosis and decreases rapidly as RBCs move away from the stenosis. Particularly, for a pair of stiffer RBCs with the initial inclination angle of 90°, the maximum value of the flow resistance is larger; while a higher flow resistance can also come from a stronger aggregation. For a pair of stiffer RBCs moving parallel to the main flow, when their positions are closer to the vessel wall at the upstream of the stenosis, the flow resistance increases due to the migration to the vessel center at the stenosis. In addition, for a

pair of RBCs with the initial inclination angle of 0°, the flow resistance from the aggregate formed by a pair of RBCs with a larger deformation is higher.

Key words: Dissipative particle dynamics · red blood cells · intercellular interaction · deformation and aggregation · flow resistance

1. Introduction

Many important biological phenomena involve the aggregation of cells. During hematogenous metastasis, cancer cells often flow through the blood stream as aggregates. Platelets form aggregates to promote blood clotting [1]. RBCs tend to aggregate to form the stacks-of-coins-like rouleaux under low shear forces and the aggregates can be reversibly broken into smaller aggregates or individual cells with the increase of shear forces. However, massive rouleaux can dramatically increase effective blood viscosity and hence impairs blood flow through small blood vessels such as microvessels. Experimental evidence showed that the older RBCs exhibit a significantly greater degree of aggregation compared to the younger ones [2]. Elevated aggregation is often associated with a higher risk of cardiovascular diseases, and occurs after myocardial infarcts, ischemic brain infarcts, in diabetes, and during sepsis [3].

In *vivo* studies demonstrated that RBC aggregation is usually modified by introducing large proteins and/or high molecular weight polymers into the blood circulation [4]. Although the exact physical mechanism of aggregation is not yet clear, two molecular models based on bridging mechanism [5] and depletion mechanism [6] have been proposed to describe RBC aggregation. The former assumes that macromolecules, such as fibrinogen and dextran, can be absorbed onto adjacent cell surfaces and bridge them together. The depletion model attributes the aggregation to a lower localized protein or polymer concentration near the cell surface than

the surrounding medium, developing a polymer depletion layer and thus leading to a decrease in osmotic pressure. These models are in qualitative and quantitative agreement with experimental measurements of cell-cell affinity and RBC aggregation induced by two types of polymers, dextran and ethylene glycol. Both of the models have assumed that an attractive force would occur when the surfaces of adjacent cells become close, and a repulsive interaction would come up when the gap between the cells is sufficiently small. Bagchi et al. [1] described the intercellular interaction through a ligand-receptor binding model and investigated the dynamics of the aggregate in a shear flow. Liu et al. [7] adopted the Morse potential to represent the interactional energy among two adjacent cells based on depletion-mediated RBC aggregation model [6] and employed this model to study the de-aggregation of RBC rouleaux at different shear rates and analyze the transport of healthy and sickle RBCs in microvessels. Recently, another mechanism of mediated intercellular interaction based on free energy minimization was proposed by Lokar et al. [8], which described the β_2-glycoprotein I (β_2-GPI) induced electrostatic interaction between the surfaces of the two RBCs by two electrical double layers.

A number of numerical studies have been carried out on the behavior of RBC aggregation in simple flows. Wang et al. [9] investigated the aggregation and dissociation of RBC rouleaux in shear and Poiseuille flows and found that the behavior of individual cells depends on factors such as intercellular interaction strength, shear stress and the deformability of the cell membrane. Li et al. [10] and Ye et al. [11] showed that the two-dimensional equilibrium configuration of the two RBCs in the static blood plasma and the mixed healthy and malaria-

infected RBCs are easily to form a rouleaux. This rouleaux is hardly disaggregated in a tube flow due to the strong intercellular interaction at a high capillary number. Without intercellular interaction, Shi et al. [12] revealed that in the Poiseuille flow, the hydrodynamic viscous force, the RBC shape and the relative locations of cells have significantly larger effects on the deformation of the leading cell than that of the rear one. Although the microvessel stenosis induces many critical diseases, only a few studies have been conducted on the flow of RBCs through the stenosis in a microvessel with a diameter comparable to the size of the RBC. Clinical findings have shown that hypertension is associated with the luminal narrowing [13]. Vahidkhah and Fatouraee [14] demonstrated that increasing the intercellular adhesion strength can lead to the formation of cell aggregates after the RBCs pass through the stenosis. Xu et al. [15] revealed that ten RBCs with stronger intercellular interaction strength might result in higher flow resistance at the stenosis. Due to the high computational cost, most of the existing studies are limited to two-dimensional simulations. In fact, when the width of a two-dimensional channel is equal to the diameter of a circular tube, the hydraulic diameter for the former is nearly two times of the latter. For laminar flows, as the Darcy friction factor is inversely proportional to the hydraulic diameter, the smaller hydraulic diameter in circular tube leads to a larger flow resistance. .

Therefore, in this study, we focus on the motion of two three-dimensional deformable RBCs in a stenosed microvessel. Firstly, the numerical method, dissipative particle dynamics, and the spring-network based RBC model coupled with the cell aggregation model are introduced in detail. Next, the equilibrium shapes of the RBC-rouleaux exerted by the

intercellular interaction with different strengths under a quasi-steady condition are numerically investigated and compared with the previous work. Then the deformation and aggregation of two RBCs passing through the stenosis are simulated and the effects of intercellular interaction strengths, cell mechano-properties and initial orientations of RBCs on the flow resistance are discussed. Lastly, summary and conclusions are presented.

2. Mathematical formulation and numerical model

2.1 Dissipative Particle Dynamics (DPD)

DPD is a mesoscopic particle-based simulation method introduced by Hoogerbrugge and Koelman [16], connecting the molecular and continuum scales. The DPD system can be thought of as a coarse-grained molecular dynamics model, where each particle represents a molecular cluster rather than an individual atom. It can access to larger time and length scales than what in the molecular dynamics. The DPD particle of mass m_i, position $\mathbf{r}_i$ and velocity $\mathbf{v}_i$ interacts with its neighboring particle *j* through three forces: conservative ($\mathbf{F}_{ij}^{\mathrm{C}}$), dissipative ($\mathbf{F}_{ij}^{\mathrm{D}}$), and random ($\mathbf{F}_{ij}^{\mathrm{R}}$) forces given by

$$\begin{aligned} \mathbf{F}_{ij}^{\mathrm{C}} &= \mathrm{F}_{ij}^{\mathrm{C}}(\mathrm{r}_{ij})\hat{\mathbf{r}}_{ij}, \\ \mathbf{F}_{ij}^{\mathrm{D}} &= -\gamma\omega^{D}(\mathrm{r}_{ij})(\mathbf{v}_{ij}\cdot\hat{\mathbf{r}}_{ij})\hat{\mathbf{r}}_{ij}, \\ \mathbf{F}_{ij}^{\mathrm{R}} &= -\sigma\omega^{R}(\mathrm{r}_{ij})\cdot\frac{\xi_{ij}}{\sqrt{dt}}\cdot\hat{\mathbf{r}}_{ij}, \end{aligned} \tag{1}$$

where $\hat{\mathbf{r}}_{ij} = \mathbf{r}_{ij}/r_{ij}$, $\mathbf{r}_{ij} = \mathbf{r}_i - \mathbf{r}_j$ and $\mathbf{v}_{ij} = \mathbf{v}_i - \mathbf{v}_j$. The coefficients γ and σ reflect the strength of dissipative and random forces, respectively. In addition, ω^D and ω^R are distance-dependent weight functions, and ξ_{ij} is a normally distributed random variable with zero mean, unit variance, and $\xi_{ij} = \xi_{ji}$. All forces are truncated beyond the cutoff radius r_c. The conservative force is given by

$$F_{ij}^{C}(r_{ij}) = \begin{cases} a_{ij}(1 - r_{ij}/r_c) & for \quad r_{ij} \le r_c, \\ 0 & for \quad r_{ij} > r_c, \end{cases} \tag{2}$$

where a_{ij} is the conservative force coefficient between particles i and j.

The random and dissipative forces form a thermostat and must satisfy the fluctuation-dissipation theorem in order for the DPD system to maintain the equilibrium temperature T [17]. This leads to:

$$\omega^{D}(r_{ij}) = \left[\omega^{R}(r_{ij})\right]^2, \qquad \sigma^2 = 2\gamma k_B T, \tag{3}$$

A generalized form for the weight functions has been proposed by Fan et al. [18].

$$\omega^{D}(r_{ij}) = \begin{cases} (1 - r_{ij}/r_c)^s & for \quad r_{ij} \le r_c, \\ 0 & for \quad r_{ij} > r_c, \end{cases} \tag{4}$$

The viscosity of a simple DPD system consists of two parts: one is the contribution from the diffusion motion of particles and another is from the dissipative forces [19]. Following the Groot and Warren's method, the radial pair distribution function g(r)=1.0 is assumed, which simplifies analysis and leads to the approximate results comparable to those derived by using a more sophisticated technique. The dissipative part of the viscosities is dominant and denoted by μ^{D}. For the above weight function, the expression can be obtained

$$\mu^{D} = \frac{2\pi\gamma\rho^2 r_c^5}{15}\left(\frac{1}{s+1} - \frac{4}{s+2} + \frac{6}{s+3} - \frac{4}{s+4} + \frac{1}{s+5}\right) \tag{5}$$

where $\rho = mn$ and n is the number density of the simulation system , the mass of one dissipative particle m is 1. The kinetic contribution to the viscosity is

$$\mu^{k} = \frac{3k_B T(s+1)(s+2)(s+3)}{16\pi\gamma r_c^3} \tag{6}$$

As $s = 0.5$ was adopted in this study, the approximate expression for the viscosity is,

$$\mu = \mu^k + \mu^D = \frac{315k_BT}{128\pi\gamma r_c^3} + \frac{512\pi\gamma n^2 r_c^5}{51975} \tag{7}$$

The time evolution of velocities and positions of particles is determined by the Newton's second law of motion

$$\begin{aligned} d\mathbf{r}_i &= \mathbf{v}_i dt \\ d\mathbf{v}_i &= \sum_{j\neq i}\left(\mathrm{F}_{ij}^C + \mathrm{F}_{ij}^D + \mathrm{F}_{ij}^R\right)dt + \mathbf{F}_{ext}dt \end{aligned} \tag{8}$$

where $\mathbf{F}_{ext}$ is the external force acting upon on the particle *i,* including the membrane force due to the cell deformation, the intercellular interaction force and the body force.

The above equations of motion are integrated using the modified velocity-Verlet algorithm[19]

$$\begin{aligned} &\mathbf{r}_i(t+\Delta t) = \mathbf{r}_i(t) + \Delta t\mathbf{v}_i(t) + \frac{1}{2}(\Delta t)^2\mathbf{f}_i(t) \\ &\tilde{\mathbf{v}}_i(t+\Delta t) = \mathbf{v}_i(t) + \lambda\Delta t\mathbf{f}_i(t) \\ &\mathbf{f}_i(t+\Delta t) = \mathbf{f}_i(\mathbf{r}_i(t+\Delta t), \tilde{\mathbf{v}}_i(t+\Delta t)) \\ &\mathbf{v}_i(t+\Delta t) = \mathbf{v}_i(t) + \frac{1}{2}\Delta t[\mathbf{f}_i(t) + \mathbf{f}_i(t+\Delta t)] \end{aligned} \tag{9}$$

where $\tilde{\mathbf{v}}_i(t+\Delta t)$ is the prediction of the velocity at time $t+\Delta t$ and λ is an empirically introduced parameter, which accounts for the additional effects of the stochastic interactions, and is set to 0.65. The velocity is first predicted to obtain the force and then corrected in the last time step.

2.2 3-D coarse-grained network model for the RBC membrane

It has been suggested that an elastic energy stored in the membrane components has a minimum when the RBC is in discocyte state and that local components of the membrane are not constrained in the biconcave resting shape [20-22]. Therefore, a healthy unstressed RBC has a biconcave equilibrium shape with the minimum energy and is described by

$$z = \pm D_0 \sqrt{1 - \frac{4(x^2 + y^2)}{D_0^2}} \left[a_0 + a_1 \frac{x^2 + y^2}{D_0^2} + a_2 \frac{(x^2 + y^2)^2}{D_0^4} \right] \tag{10}$$

where $D_0 = 7.82$ μm is the average diameter, $a_0 = 0.0518$, $a_1 = 2.0026$, and $a_2 = -4.491$. The membrane network structure is generated by triangulating the unstressed equilibrium shape described by Eq. (10). The membrane is discretized into a number of triangle elements formed by a series of vertices. The coordinates of vertices are regarded as the initial positions of the membrane particles. Figure 1 shows the network model of a RBC, the vertices are connected by wormlike springs.

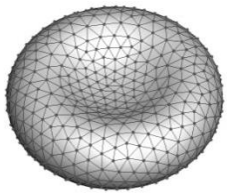

Fig. 1 The network model of a RBC

The total energy of the network consists of the in-plane elastic energy, the bending energy, the surface area energy, and the volume energy [23-25]. In our previous study[26], this model was used to simulate the deformation of a tumor cell passing through a narrow slit. The in-plane elastic energy for the WLC-POW model is given by

$$E_{in-plane} = \sum_{all\,edges} \left[\frac{k_B T l_{\max}}{4p} \frac{3x_l^{\,2} - 2x_l^{\,3}}{1 - x_l} + \frac{k_p}{(m-1) l^{m-1}} \right] \tag{11}$$

where $x_l = l / l_{\max} \in (0,1)$, $l_{\max}$ is the maximum spring extension, which is equal to 2.2 times equilibrium spring length for the WLC model, p is the persistence length, k_B is Boltzmann constant and T is temperature of the system. k_p is a POW force coefficient and m is a specified exponent, which is set to 2 [27].

The bending energy is concentrated at the element edges according to the bending potential

$$E_{bending} = \sum_{all\ triangle\ adjacents} k_{bend}\left[1-\cos(\theta_i - \theta_0)\right] \tag{12}$$

where k_{bend} is the bending modulus; θ_i is the instantaneous angle formed between the outer normal vectors of two adjacent triangles α, β sharing the *i*th edge; θ_0 is the spontaneous angle.

The area and volume conservation constraints are presented as follows:

$$E_{area} = \frac{k_{area}^{tot}(A - A_0^{tot})^2}{2A_0^{tot}} + \sum_{all\ triangles} \frac{k_{area}(A_j - A_0)^2}{2A_0} \tag{13}$$

$$E_{volume} = \frac{k_{volume}(V - V_0^{tot})^2}{2V_0^{tot}} \tag{14}$$

where k_{area}^{tot} , k_{area} and k_{volume} are constraint constants for the global area, local area, and volume; N_t is the number of the triangle elements; A and V are the instantaneous membrane area and the cell volume, respectively; A_0^{tot} and V_0^{tot} are their respective specified total area and volume values. A_j, A_0 are the instantaneous and initial local areas.

The elasticity of the network is based on a linear analysis of a two-dimensional sheet of springs built with equilateral triangles. The linear shear modulus of the WLC-POW model is

$$G = \frac{\sqrt{3}k_B T}{4pl_{\max}x_0}\left(\frac{x_0}{2(1-x_0)^3} - \frac{1}{4(1-x_0)^2} + \frac{1}{4}\right) + \frac{\sqrt{3}k_p(m+1)}{4l_0^{\,m+1}},\ x_0 = l_0 / l_{\max} \tag{15}$$

where l_0 is the equilibrium spring extension.

The linear area compression modulus is defined as

$$K = 2G + k_{area}^{tot} + k_{area} \tag{16}$$

The Young's modulus Y for the two-dimensional sheet can be expressed as a function of the shear and area-compression moduli as follows

$$Y = \frac{4KG}{K+G} \tag{17}$$

The relationship between bending modulus k_{bend} and the macroscopic membrane bending rigidity k_c is derived for the case of a spherical shell with the Helfrich bending energy, which is expressed by:

$$k_{bend} = \frac{2}{\sqrt{3}} k_c \tag{18}$$

2.3 RBC aggregation model

To analyze the RBC aggregation, we adopted the depletion model proposed by Liu et al. [7]. In this model a Morse potential function $\psi(r)$ is used to model the interaction energy

$$\psi(r) = D_e[e^{2\beta(r_0-r)} - 2e^{\beta(r_0-r)}] \tag{19}$$

where r is the distance between two plane elements of the opposing RBCs directly facing each other, r_0 is the zero force length, D_e is the intercellular interaction strength, and β is the scaling factor controlling the interaction decay behavior. Therefore, the total interaction energy [11] of a triangulated cell is expressed by

$$\psi(\{\mathbf{r}_i\}) = \sum_{j=1,N_t} \psi(r_{jk})(\mathbf{n}_j \cdot \mathbf{I}_j)(\mathbf{n}_k \cdot \mathbf{I}_k)A_j \tag{20}$$

where r_{jk} is the local distance between the jth and kth triangles located in cells 1 and 2 respectively. $\mathbf{n}_j$ and $\mathbf{n}_k$ are the outward unit normal vectors to the those curved elements, $\mathbf{I}_j$ and $\mathbf{I}_k$ stand for the unit vectors parallel to the line joining the centers of two cells and directed toward each other, which are based on the DLVO (Derjaguin-Landau-Verwey-

Overbeek) theory [28] to describe the interaction energy between two curved surfaces. A_j is the area of *j*th triangle of cell 1. The interaction force acting on the membrane particle *i* on the surface of cell 1 is given by:

$$f_i^{agg} = -\frac{\partial \psi(\{\mathbf{r}_i\})}{\partial \mathbf{r}_i} \tag{21}$$

The intercellular interaction force is simply illustrated as a weak attractive force at a far distance, but a strong repulsive force at a near distance. In the numerical model, in order to save the computational cost, a cut-off distance r_c^{agg} is defined as a zero force separation threshold and set to be 3.52, exceeding which the intercellular force is assumed to be zero.

2.4 Model and physical unit scaling

The scaling procedure [27] has been presented, which relates the model's non-dimensional units to the physical units. In order to keep the simulation system consistent with the real system, the physical properties should be mapped onto the dimensionless properties in the model. The length scale is adapted as:

$$L^S = \frac{D_0^P}{D_0^M} \tag{22}$$

where the superscript M and P denote "model" and "physical". The energy scale is provided as follows,

$$E^S = \frac{Y^P}{Y^M}\left(\frac{D_0^P}{D_0^M}\right)^2 \tag{23}$$

The force scale is defined by

$$N^S = \frac{Y^P}{Y^M}\frac{D_0^P}{D_0^M} \tag{24}$$

The scaling between the model and physical times is defined as follows

$$\tau^S = \frac{Y^M}{Y^P}\frac{D_0^P}{D_0^M}\frac{\mu^P}{\mu^M} \tag{25}$$

3. Results and Discussion

In the present study, the blood plasma is considered as an incompressible Newtonian fluid and the cytoplasm has the same density as the blood plasma. The modeling parameters are listed in Table 1. The number density of the fluid particles in simulation system is set to be 6 and the membrane for each cell consists of 640 particles. No-slip boundary condition is applied at the wall and to simulate a pressure-driven flow, periodic boundary condition is imposed between the entrance and the exit of the channel or the stenosed microvessel.

Table 1 Simulation parameters

Parameter	Simulation	Physical values
Blood plasma density (ρ)	6	$1.0\times10^3\,\mathrm{kg/m^3}$ [29]
Blood plasma viscosity (μ)	102.5	$1.2\times10^{-3}\,\mathrm{Pa\cdot s}$ [29]
Temperature (T)	0.08486	310K
Membrane shear modulus (G)	94~906	$6.3\sim60\mu\mathrm{N/m}$ [30]
Membrane bending modulus (k_{bend})	4.565	$2.3\times10^{-19}\,\mathrm{J}$ [27]
Intercellular energy density (D_e)	1.976~88.92	$0.1\sim4.5\mu\mathrm{J/m^2}$ [9, 10]
Scaling factor (β)	3.84	$3.84\mu\mathrm{m^{-1}}$ [31]
Zero force distance (r_0)	0.49	$0.49\mu\mathrm{m}$ [31]
Time step (Δt)	0.0005	$8.73\times10^{-5}\,ms$
Global area constraint constant(k_{area}^{tot})	5×10^4	$3.35\times10^{-3}\,\mathrm{N/m}$
Local area constraint	100	$6.7\mu\mathrm{N/m}$

constant(k_{area})		
Volume constraint constant(k_{volume})	5×10^{4}	$3.35\times10^{-3}\,\mathrm{N/m}$
Cut-off radius(r_c)	1.25	1.25μm

3.1 Validation

To validate the aggregation model combined with three-dimensional network membrane model, two biconcave-shaped healthy RBCs with intercellular forces were placed in a three-dimensional channel. The fluid domain is $20\times20\times20\,\mu m^3$, and the initial distance between the centers of the two RBCs was $3.1\,\mu m$. In order to compare with the previous numerical results, the viscosity ratio of cytoplasm to the plasma is set to 1. Figure 2 illustrates the equilibrium cell shapes of three-dimensional RBC rouleaux in the static blood plasma under different intercellular interaction strengths, (e) $D_e = 0\,\mu J/m^2$; (f) $D_e = 0.1\,\mu J/m^2$; (g) $D_e = 1\,\mu J/m^2$; (h) $D_e = 4.5\,\mu J/m^2$ and the results were compared with Wang et al. [9] and Li et al. [10], as shown in Figs. 2a, b, c and d.

When there is no cell-cell adhesion, cell keeps its initial biconcave shape. Once the intercellular interaction force is applied on the adjacent cells, the RBCs move toward each other until the attractive force and the repulsive force reach equilibrium state. The equilibrium configuration was obtained when the intercellular interaction force was balanced with the membrane constraint forces which control the cell deformation. If intercellular interaction strength is strong enough, the contact surfaces of the two cells become flat and the distance between the contact surfaces remains nearly zero force distance. The shape of noncontact surfaces of two cells varies with the intercellular interaction strength. The cells display concave

shapes at weak intercellular interaction strength ($D_e = 0.1\mu J/m^2$), flattened shapes at moderate intercellular interaction strength ($D_e = 1\mu J/m^2$), and convex shapes at strong intercellular interaction strength ($D_e = 4.5\mu J/m^2$). The contact area increases with the intercellular interaction strength that is due to the fact that at the high intercellular interaction strength, the intercellular interaction force can overcome the constraint force and change the cell shape. In addition, it can be observed that the present results are in a good agreement with two-dimensional equilibrium configuration of RBC rouleaux reported by Wang et al. [9] and Li et al. [10].

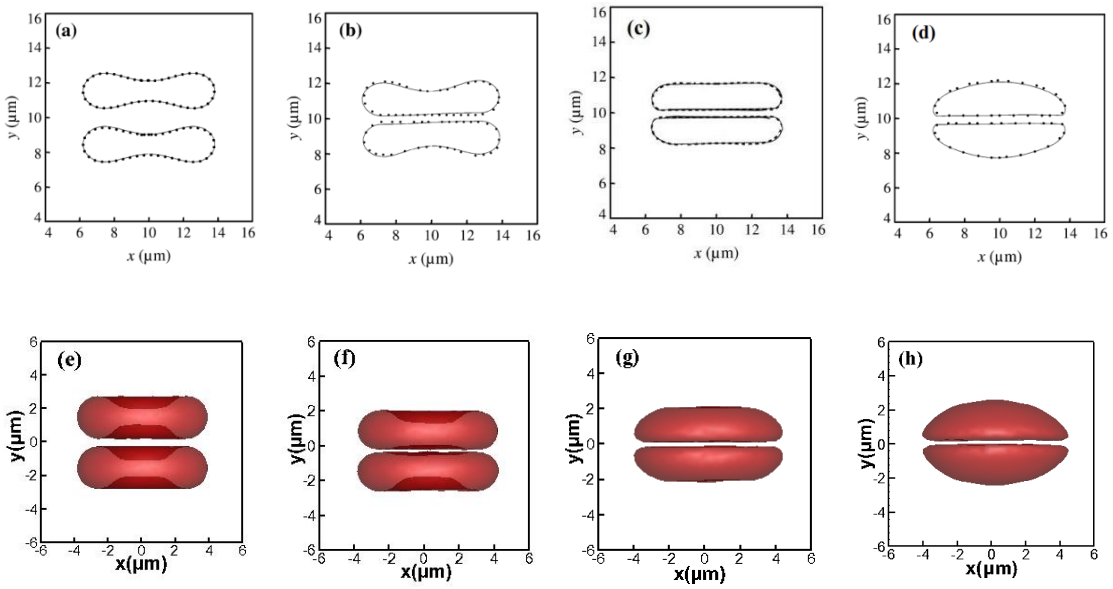

Fig. 2 Equilibrium configuration of RBC rouleaux at different intercellular interaction strengths. (a) and (e) $D_e = 0\mu J/m^2$; (b) and (f) $D_e = 0.1\mu J/m^2$; (c) and (g) $D_e = 1\mu J/m^2$; (d) and (h) $D_e = 4.5\mu J/m^2$. Solid lines and black dot lines in (a), (b) and (d) represent the simulation results reported by Wang et al. [9] and Li et al. [10] respectively. Dash line in (c) is reported by Wang et al. [9]. (e)-(h) are the present simulation results.

3.2 Fluid flows without RBCs in a straight microvessel and a stenosed microvessel

In this section, we first performed the simulation of a Poiseuille flow in a straight tube with 50μm in length and 12μm in diameter. In the DPD model, a uniform dimensionless body force $f_y = 1.125$ was applied to the solvent particles in the flow direction. Such an applied force is equivalent to the pressure gradient $\Delta P / L = \rho f_y$, where ΔP is the pressure drop over the tube length L and ρ is the suspension's mass density. The fluid viscosity according to its approximate expression equation (7) can be calculated as 102. In order to make a comparison with the macro-Poiseuille flow model, the analytic solution for the profile of flow velocity along the diameter of cross section is given by $v_y(r) = \rho f_y(R^2 - r^2)/4\mu$. Figure 3 compares the simulation result with the analytic solution in the macro-Poiseuille flow model. It can be found that the velocity distribution is in good agreement with the theoretical values. So the Reynolds number is $Re = \rho u_m D / \mu = 0.21$, where u_m is the mean velocity of the flow. It is larger than the typical value ($Re = 0.03$) for the arterioles with a diameter of 15μm and is one to two orders of magnitude higher than the values for the venules and capillaries [3]. In fact, the calculated physiological Re is based on the mean flow velocity and the bulk viscosity of blood at 45% hematocrit. Under the fixed pressure drop, the mean flow velocity decreases by more than 50% at the hematocrit of 45% in comparison with that for the flow in the absence of RBCs [32] while the bulk viscosity of blood at 45% hematocrit is nearly 3 times that of the plasma. Therefore, the Re for the flow without RBCs in the present study may be nearly 6 times larger than that for the blood flow at 45% hematocrit under the same pressure drop, which is approximate to the Re for the arterioles $f_y = 1.125$ assures $Re = 0.21$..

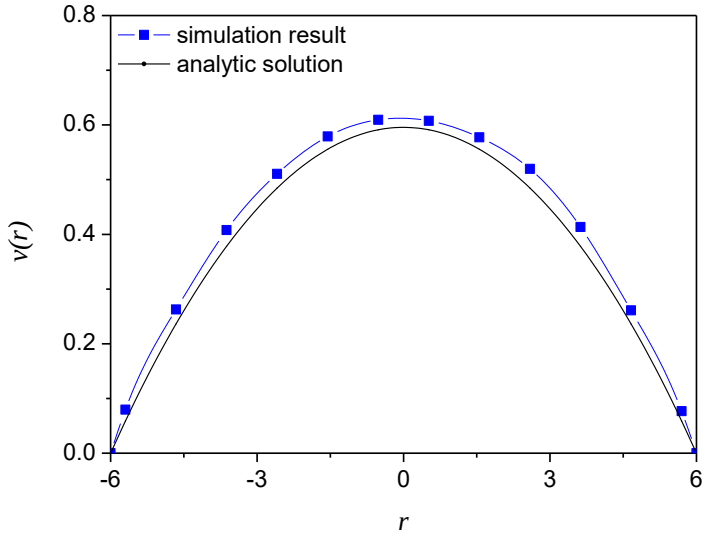

Fig. 3 Velocity profiles for the Poiseuille flow in a straight microvessel driven by a body force

$$f_y = 1.125$$

Next, the fluid flow in the absence of RBCs in a microvessel with a stenosis under the same flow condition as the Poiseuille flow in the straight microvessel was simulated. Here, the stenosis is 8μm long and has a minimum diameter of 8μm. Figure 4 illustrates the distribution of velocity vectors and contours for the cross section of the flow without RBCs in a stenosed microvessel. It shows that the flow velocity reaches its maximum in the stenosed zone and there is no separation in the downstream region of the stenosis at such a low Reynolds number.

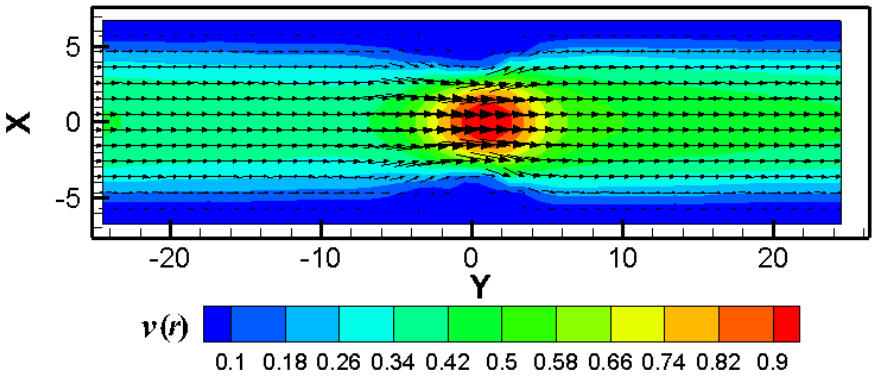

Fig. 4 The distribution of velocity vectors and velocity magnitude contours for the cross section of the flow without RBCs in a stenosed microvessel

3.3 Two RBCs in a stenosed microvessel

In this section, two healthy RBCs moving in a stenosed microvessel was simulated and compared with their counterparts in the straight microvessel. The initial distance between the two RBCs was set to be 3.1μm, as shown in Fig 5a, and the intercellular interaction strength is 0.5μJ/m^2 to produce an attractive force. The membrane shear modulus for the healthy RBC is 6.3μN/m. The viscosity of hemoglobin solution was measured by Cokelet and Meiselman [33], yielding a range of 3~10×10^{-3}Pa•s for the physiologically relevant concentration of hemoglobin. Here, the RBC is filled with a fluid of the viscosity of 6×10^{-3}Pa•s similar to the RBC cytosol which is a hemoglobin solution. Since the motion, deformation and aggregation of two RBCs are complex processes depending on the hydrodynamic viscous force, the intercellular interaction force and the elasticity of the membrane, it is thus necessary to introduce some dimensionless groups: Re, Ca and G_I. Re is the Reynolds number. $Ca = \mu u_m / G$ is the capillary number, implying the relative importance of the hydrodynamic viscous forces to the membrane shear deformation, and it is calculated as $Ca = 0.32$ in the straight microvessel. The dimensionless group $G_I = D_e / G$ determines the relative importance of the intercellular interaction to the membrane shear deformation.

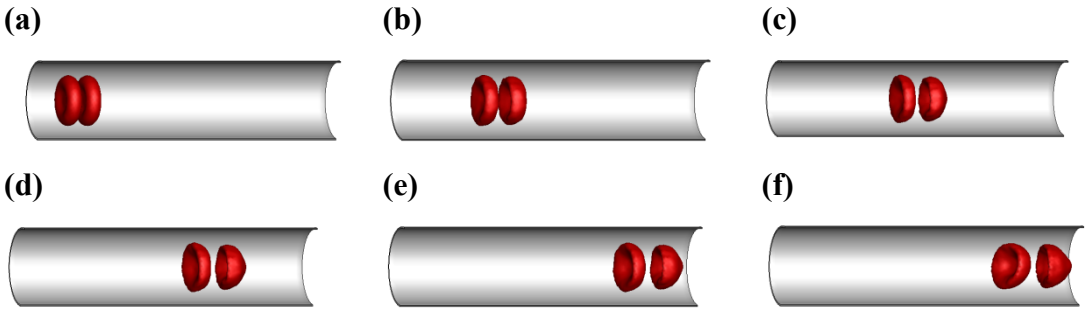

Fig. 5 Deformation and motion of two healthy RBCs in a straight microvessel at t = 0.0, 21.5, 41.5, 61.5, 81.5, 197.5

In the straight microvessel, as the viscosity ratio is larger compared to the numerical studies conducted by Ye et al. [11], all the cells deform gradually from the concave shape to the parachute shape initially, as shown in Figs. 5a~5e. The deformation of the two RBCs are increasingly affected by the hydrodynamic viscous force instead of the aggregation force, indicating that the RBC aggregates cannot be formed when subjected to a weak intercellular interaction force, as shown in Fig. 5f. The leading cell experiences larger deformation than the rear one in the flow. When the two RBCs flow in the stenosed microvessel, they are significantly stretched when passing through the stenosis, as illustrated in Figs. 6c-6e. Since the flow velocity in the stenosed area increases quickly, the capillary number grows considerably. However, after the stenosis, the RBCs tend to recover from parachute type to concave shape with the decrease in the flow velocity.

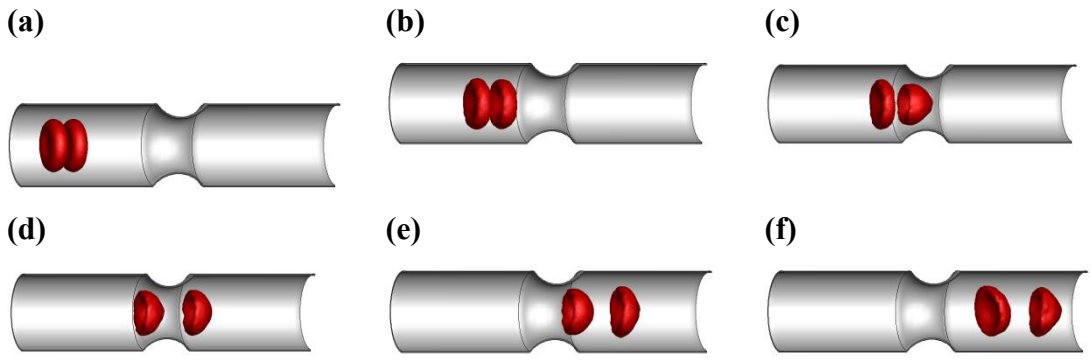

Fig. 6 Deformation and motion of two healthy RBCs flowing in a stenosed microvessel at t = 0.0 (a), 21.5 (b), 41.5 (c), 61.5 (d), 81.5 (e), 247.5 (f).

To evaluate the effects of stenosis and RBCs on the flow, the relative flow resistance R was introduced, which is defined by

$$R = \frac{f_{RBC}^{D}}{f_{0}^{D}} \tag{26}$$

where f^D is the Darcy's friction factor which is defined as $f^D = 64/Re = 64\mu/\rho u_m D$ for laminar flow in a circular tube, and the subscripts "RBC" and "0" denote flow with RBC and without RBC, respectively. Figure 7 presents the trajectories of two RBCs and the evolution of relative flow resistance when two RBCs move in the stenosed microvessel. In addition, the time-averaged flow resistance for the flow without RBCs in the presence of stenosis and the flow with RBCs in a straight microvessel were also plotted in Fig. 7, respectively. The instantaneous relative flow resistance increases greatly when the leading RBC enters into the stenosis and reaches its first peak when the leading RBC arrives at the center of the stenosis. Following that, it experiences a dramatic downward trend because the leading RBC is leaving from the stenosis while the trailing one has not entered into the stenosis completely. Until the leading RBC leaves away thoroughly, the flowing resistance drops to its valley value. Then its second peak occurs when the trailing RBC gets to the center of the stenosis. After both of the two RBCs pass through the stenosis, the flow resistance falls nearly to the average value for the blood plasma flow in the stenosed microvessel. Moreover, it also indicates that the narrowing due to the stenosis results in a significantly increase in the flow resistance. Particularly, the presence of stenosis leads to the increase of approximate 30% in the flow resistance by comparing the flow of RBCs in the stenosed and straight microvessels.

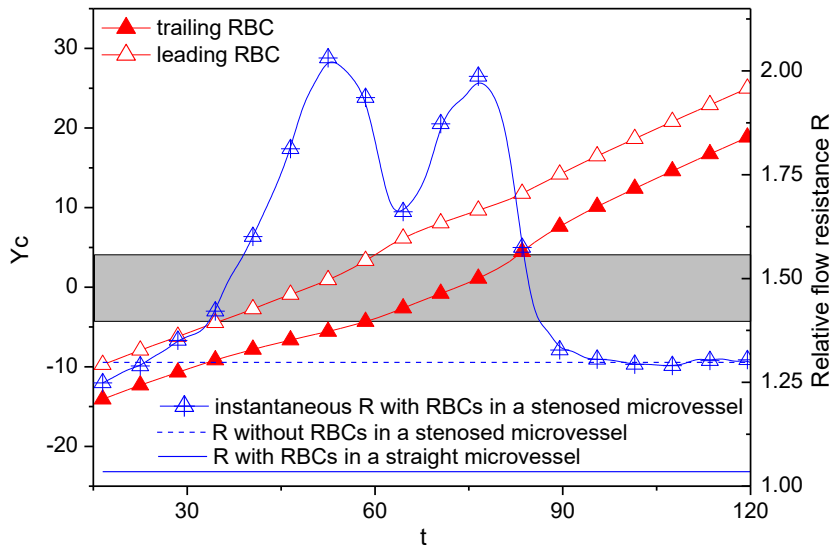

Fig. 7 Trajectories of two RBCs in a stenosed microvessel and the corresponding instantaneous relative flow resistance, where *Yc* represents the mass center of the RBC along the flow direction.

3.4 Effects of RBC membrane elasticity and intercellular interaction strength

Experimental evidence [30] showed that the elastic shear modulus of the malaria infected RBCs at the ring, trophozoite and schizont stages ranges from 15 to 60 $\mu N/m$. The effects of the membrane elasticity and the weak aggregation interaction on the deformation of the two RBCs with $D_e = 0.5 \mu J/m^2$ were investigated by comparing the deformation of a pair of RBCs with three different elastic shear moduli G=6.3μN/m, 25μN/m and 60μN/m and the same bending modulus $k_{bend} = 2.3 \times 10^{-19} J$. The deformation index (DI) is introduced to measure the degree of cell deformation. As the membrane particles near the axis move faster than those near the wall, the difference of the axial velocity on the membrane causes the cell elongation. So DI is defined as the ratio between the axial length and radial width of the cell.

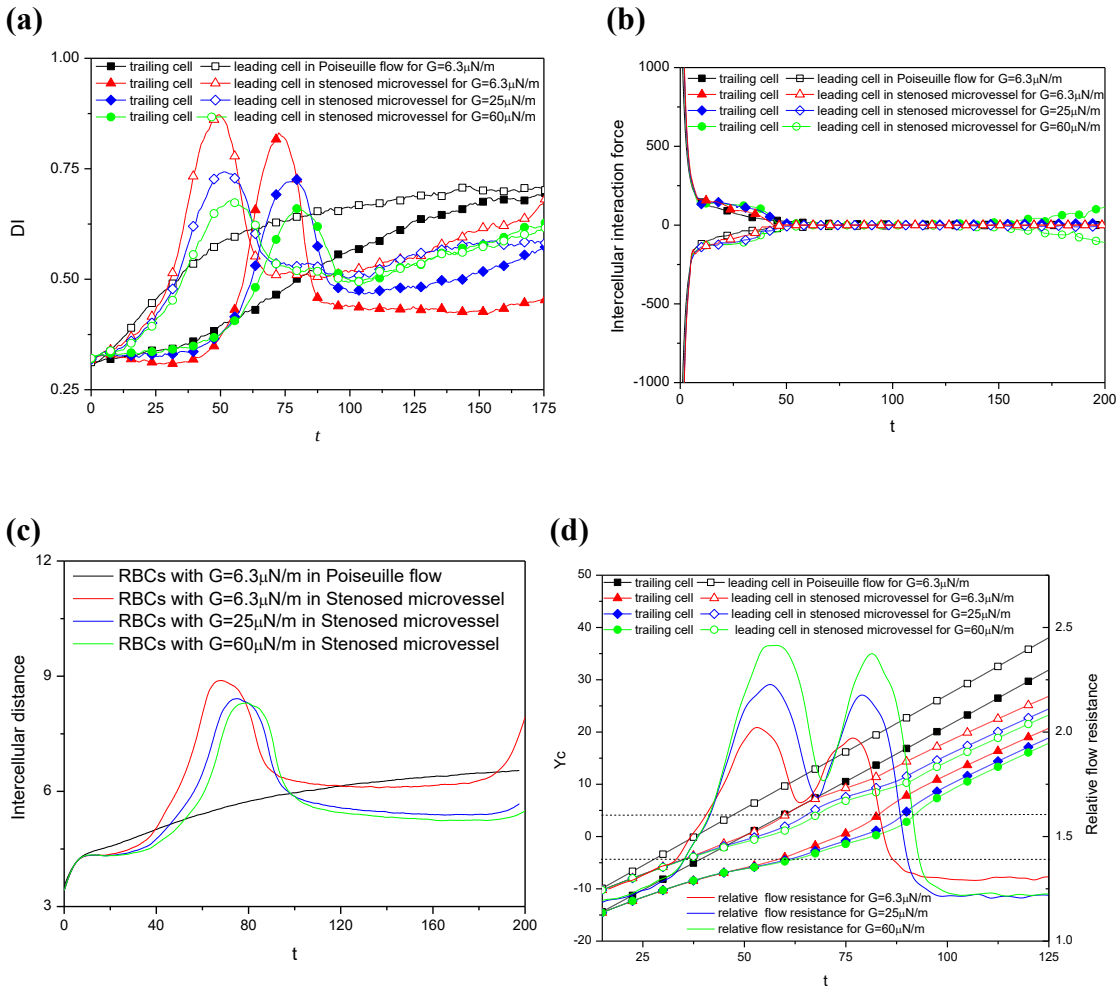

Fig. 8 (a) Evolutions of deformation indexes of two RBCs; (b) Variations of the y-component intercellular aggregation force F_y^{Int} with time t acting on two RBCs; (c) Evolutions of the distance between the centroids of two RBCs along the flow direction; (d) Trajectories of two RBCs with the shear modulus 6.3μN/m, 25μN/m and 60μN/m respectively, in a stenosed microvessel and the corresponding instantaneous relative flow resistance

In Fig. 8a, in the straight microvessel, the DI of the leading RBC is greater than that of the trailing one and its increase rate for the leading cell is larger than that for the trailing one before t = 50, but after this time, the DI of the leading cell increases slightly and the trailing one deforms extensively. This is due to the weak attractive forces (Fig. 8b) between the two

RBCs, which results in a growing intercellular distance (Fig. 8c). Consequently, the deformation is mainly affected by the hydrodynamic viscous force. Next, the deformation indexes of the two RBCs for different shear moduli in a stenosed microvessel were compared in Fig 8a. Before the leading RBC enters into the stenosis, there is a slight difference in the deformation index for different pairs of RBCs with different shear moduli. However, when passing through the stenosis, both of the two RBCs exhibits enhanced deformation and decreasing the membrane deformability weakens the RBC deformation. The deformation indexes for both the leading RBC and the trailing one are up to their maximum when they arrive at the narrowest section of the stenosis separately. Owing to the reduced flow velocity in the downstream of the stenosis, the RBC has a lower deformation index than that in the straight microvessel after it leaves away from the stenosis. It should be noted that the presence of stenosis increases the intercellular distance, especially for a pair of highly deformable RBCs. That means the formed incomplete aggregates before the stenosis may be broken when traveling through the stenosis. In addition, the stiffer pair of RBCs experiences weak deformation, indicating the RBC projected area on the cross section is comparatively large. Once the ratio of the RBC projected area to the stenosed area on the cross section perpendicular to the flow direction becomes larger due to the decreasing membrane deformability, a significant increase can be seen in the instantaneous relative flow resistance, as plotted in Fig. 8d. Specifically, decreasing the RBC membrane deformability by nearly 10 times can cause an increase of approximately 25% in the maximum flow resistance occurred when the RBC approaches the stenosis.

As the RBCs pass through the stenosis separately under the condition of $D_e = 0.5\mu J/m^2$, it is necessary to investigate how the aggregate affects the flow resistance when it gets through the stenosis. Therefore, the migration of two healthy RBCs in a stenosed microvessel for three different values of intercellular interaction strength, $D_e = 0.5, 0.8, 1\mu J/m^2$, corresponding to $G_I = 0.079, 0.127, 0.159$ respectively, was studied in terms of the evolution of the flow resistance. Increasing the intercellular interaction strength to $0.8\mu J/m^2$ and $1\mu J/m^2$ promotes the formation of a rouleaux before the stenosis and the higher D_e makes closer aggregation. The intercellular interaction force is strong enough to inhibit the dissociation of the rouleaux when it passes through the stenosis, as shown in Fig.9. The flow resistance experiences only one peak when the pair of RBCs as a rouleaux travels across the stenosis (see Fig. 10). Also, the peak value of the flow resistance caused by the rouleaux is larger than that brought by two individual RBCs. In addition, the stronger cell-cell interaction can lead to higher flow resistance at the stenosis of the microvessel.

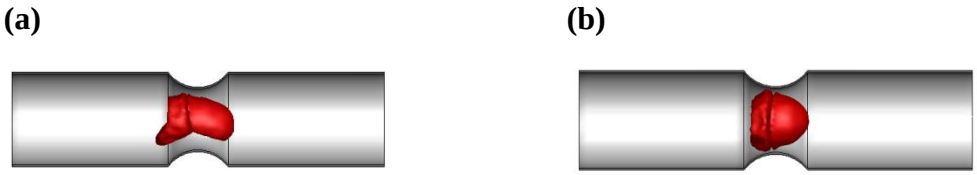

Fig. 9 Snapshot of the two RBCs passing through the stenosis for (a) $G_I = 0.127$ and (b) $G_I = 0.159$

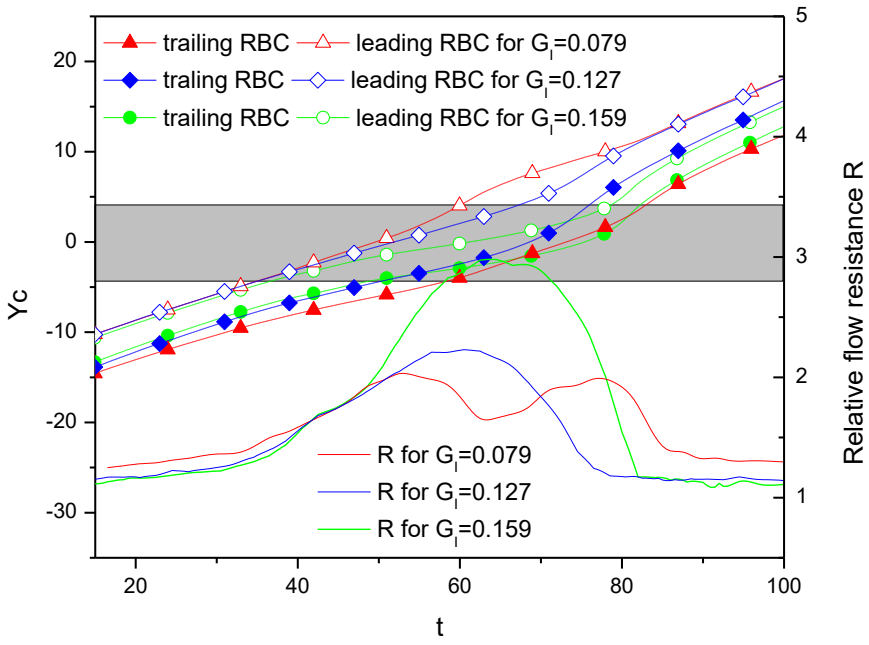

Fig. 10 Trajectories of two RBCs in the stenosed microvessel and corresponding instantaneous relative flow resistance for G_I = 0.079, 0.127 and 0.159 respectively

3.5 Effects of initial RBCs orientation

In this section, the initial RBC orientation was taken into account to investigate its effect on the aggregation of the two RBCs and the flow resistance. First of all, the initial RBC inclination angle is defined by the angle between the main flow direction and the major axis of the RBC. The initial inclination angle θ for both of the RBCs was set to 90° in the last section, which can generate a relatively high flow resistance, but here it was varied to 0°. The simulation of a pair of healthy RBCs with the intercellular interaction strength of $D_e = 0.5\mu J/m^2$ and the intercellular distance of $L_{c-c} = 3.1\mu m$ passing through the stenosed microvessel was carried out firstly. The cells are 20μm away from the center of the stenosis at the initial time. As shown in Fig. 11, there is no rouleaux formed before the stenosis and even the cells are forced to approach each other when they are passing through the stenosis. This is due to two reasons.

One is that the intercellular interaction force is relatively weak, another is that there is no sufficient time to form aggregates due to the increased velocity at the stenosis. Subsequently, the intercellular distance becomes increasingly large and the two cells flow dispersedly after they leave away from the stenosis because of the divergent fluid velocity vectors. In terms of the deformation of the RBCs, as the RBCs flow parallel to the main flow and the flow velocity increases significantly in the stenosis, little deformation is observed and only stretching deformation occurs when they are flowing in the stenosis.

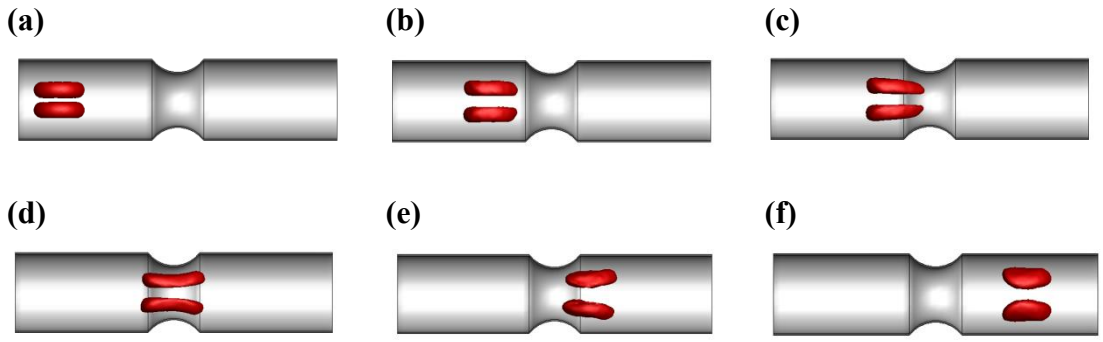

Fig. 11 Case 1: Deformation and aggregation of two RBCs with $D_e = 0.5\mu J/m^2$ for the initial intercellular distance $L_{c-c} = 3.1\mu m$ in a stenosed microvessel at different time steps: (a) *t*=0; (b) *t*=36.5; (c) *t*=57.5; (d) *t*=96.5; (e) *t*=126.5; (f) *t*=156.5

However, when the intercellular interaction strength is increased by a factor of two, the aggregate is formed before the stenosis (Fig. 12b~c) as the noncontact surfaces of the two RBCs have converted from the concave to the flat. There exists an empty gap (the dark red regions of the RBCs) between the two RBCs, so a complete aggregate has not been achieved before it passes through the stenosis. The aggregate undergoes stretching deformation owing

to the geometrical effect of the stenosis, as illustrated in Fig. 12d. After the stenosis, the divergent velocity vectors facilitate the aggregate deformation from ellipsoidal shape to a near spherical shape (Fig. 12e), which is consistent with the two-dimensional findings provided by Vahidkhah and Fatouraee [14]. With the increase in the contact time, the empty gap between the two RBCs is shortened gradually and the noncontact surfaces of the RBCs deform to the concave shape. As a decreased flow velocity occurs downstream the stenosis as shown in Fig. 4, the hydrodynamic viscous force is weaker compared with the intercellular interaction force so that the aggregate cannot be broken into the individual cells.

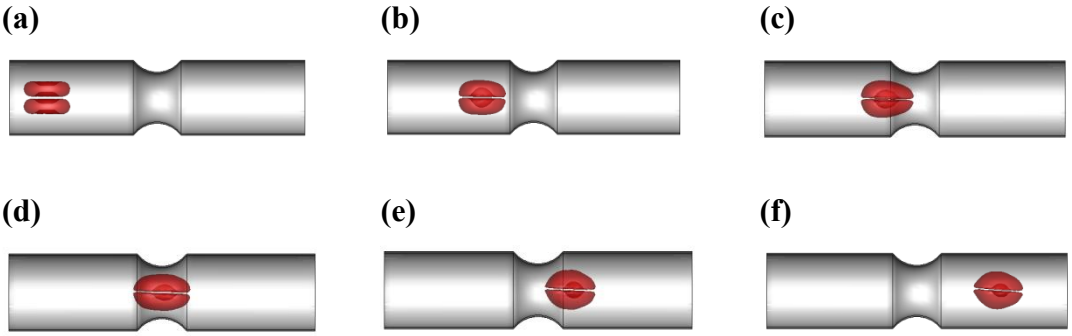

Fig. 12 Case 2: Deformation and aggregation of two RBCs with $D_e = 1\mu J/m^2$ for the initial intercellular distance $L_{c-c} = 3.1\mu m$ in a stenosed microvessel at different time steps: (a) *t*=0; (b) *t*=36.5; (c) *t*=57.5; (d) *t*=87.5; (e) *t*=108.5; (f) *t*=138.5

Next, the initial distance between the two RBCs was enlarged to 6.2μm while D_e remains to be $1\mu J/m^2$. The weak attractive force cannot promote the formation of rouleaux before the stenosis (Figs. 13b~c) due to the initial large intercellular distance. Although a strong attractive force is generated between the two RBCs when they pass through the stenosis, there is no enough contact time for them to form the aggregate even if they are forced to approach each other (Fig. 13d). After they move away from the stenosis, the deformation behavior of the two

cells are nearly same as in the first case in this section, by comparing Figs. 13d~e and Figs. 11d~e.

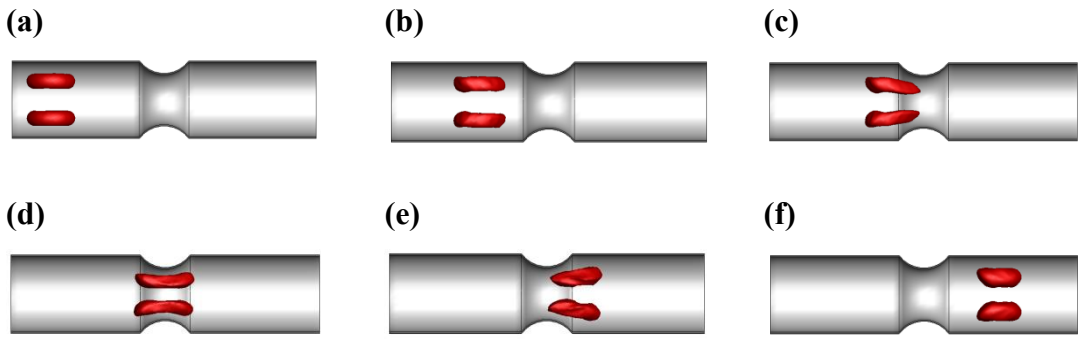

Fig. 13 Case 3: Deformation and aggregation of two RBCs with $D_e = 1\mu J/m^2$ for the initial intercellular distance $L_{c-c} = 6.2\mu m$ in a stenosed microvessel at different time steps: (a) *t*=0; (b) *t*=26.5; (c) *t*=43.5; (d) *t*=77.5; (e) *t*=97.5; (f) *t*=116.5

In the last simulation, the intercellular interaction strength for the two RBCs that are 6.2μm apart from each other initially was set to be $4.5\mu J/m^2$. The results are presented in Fig. 14. Similar results are obtained in the initial time steps as shown in Fig. 13. When the two cells get into the stenosis simultaneously, the front parts of the cells are closer to each other compared with the last case due to the strong cell-cell attractive force, as observed in Fig. 14d. As time progresses, two cells attach to each other and form a steady rouleaux which is hardly separated by the hydrodynamic viscous force, as shown in Fig. 14e~f.

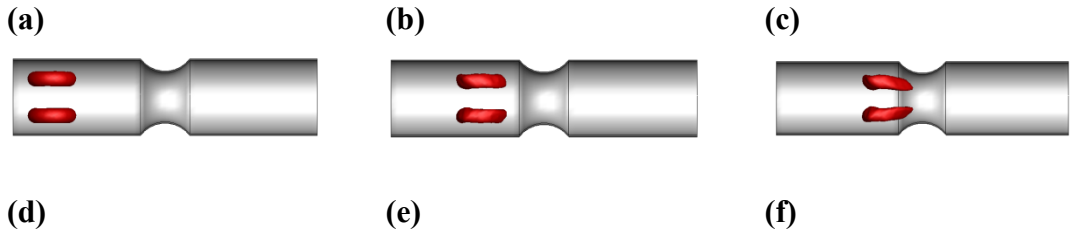

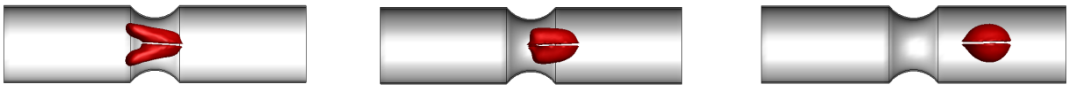

Fig. 14 Case 4: Deformation and aggregation of two RBCs with $D_e = 4.5\mu J/m^2$ for the initial intercellular distance $L_{c-c} = 6.2\mu m$ in a stenosed microvessel at different time steps: (a) *t*=0; (b) *t*=26.5; (c) *t*=43.5; (d) *t*=77.5; (e) *t*=97.5; (f) *t*=131

Finally, the time variation of the relative flow resistance and the centroid positions of the two RBCs for the above four cases were compared in Fig. 15. Noticeably, the pair of RBCs as an aggregate formed upstream (Case 2) move faster than the other cases because the aggregate moves almost along the centerline of microvessel. Fig. 15 shows that the flow resistance reaches its highest point when the two RBCs form the aggregate within the stenosis as shown in Fig. 14 (Case 4). However, for Case 2 where the aggregate forms upstream, the flow resistance is the smallest since the aggregate migrates with a larger velocity. Furthermore, by comparing the aggregate passing through the stenosis with initial inclination angle θ=90° and θ=0°, it seems that the aggregate flowing parallel to the main flow with little deformation causes less flow resistance when it reaches the stenosis.

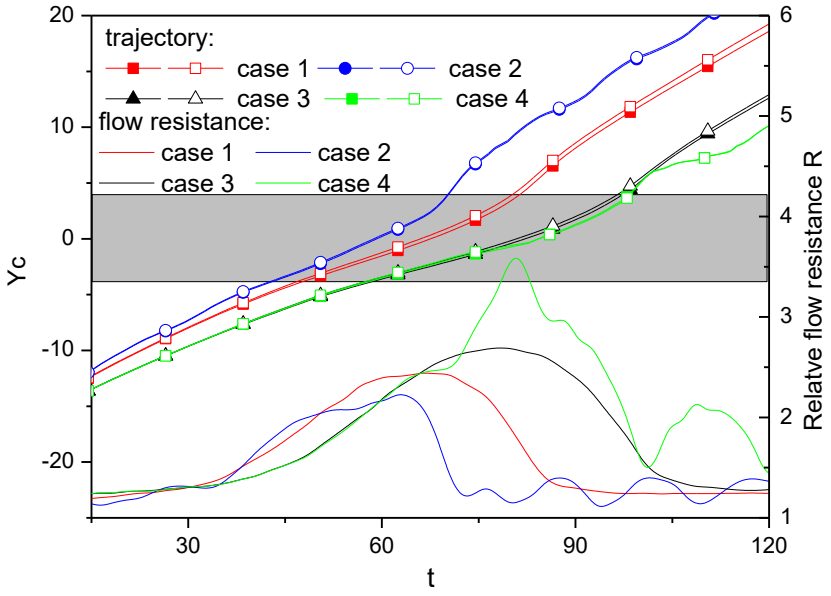

Fig. 15 Trajectories of two RBCs in a stenosed microvessel and corresponding instantaneous relative flow resistance for case 1: $G_I = 0.079, L_{c-c} = 3.1\mu m$; case 2: $G_I = 0.159, L_{c-c} = 3.1\mu m$; case 3: $G_I = 0.159, L_{c-c} = 6.2\mu m$ and case 4: $G_I = 0.714, L_{c-c} = 6.2\mu m$. The solid symbol represents the bottom RBC and the hollow one represents the upper RBC.

4. Conclusions

In summary, the behaviors of RBC deformation and aggregation in a stenosed microvessel under a quasi-steady condition were investigated numerically by using dissipative particle dynamics. A spring-based network cell model was employed to represent deformable 3D RBC membrane. The plasma was regarded as incompressible Newtonian fluid. And a Morse potential function based on depletion-mediated RBC aggregation model was used to characterize the aggregation of cells.

Firstly, the aggregation model was verified by comparing the results of equilibrium configurations of rouleaux formed under the quasi-steady condition and the action of different cell-cell interaction strengths with the previous 2D simulation results. The findings showed that

the contact surfaces between two cells deform from a concave shape to a flat shape at a higher intercellular interaction strength while the non-contact surfaces remain the concave shape at a weak cell-cell adhesion strength. With the increase in the intercellular interaction strength, they become flat and even convex at high interaction strengths. These are qualitatively similar to the previous numerical results of Wang et al. [9] and Li et al. [10].

Then, the motion of two RBCs in a stenosed microvessel was simulated. Three types of the RBC shape can be distinguished. When the RBCs with initial inclination angle of 90° pass through the stenosis, parachute shape and asymmetric slipper shape occur at the initial and later stages respectively. But when the RBCs move along the main flow direction, only extension deformation can be observed when they traverse the stenosis. The increased flow velocity at the stenosis enlarges the distance between the two RBCs with weak intercellular interaction strength for the inclination angle of 90°. For the inclination angle of 0°, there is no sufficient time for the rouleaux formation at the stenosis when the intercellular interaction is not strong enough. Both of the two RBCs passing through the stenosis separately have a higher deformation index at the stenosis due to the higher capillary number, especially for the softer ones.

Moreover, the relative flow resistance, as a measurement of the effect of the RBC behaviors on the blood flow, was calculated and analyzed. The presence of stenosis and RBCs causes a significant increase in the average flow resistance. The flow resistance increases considerably when the RBCs enter into the stenosis and decreases rapidly when they leave away from the stenosis. For a pair of RBCs with the inclination angle of 90°, the flow resistance

is significantly higher for the stiffer RBCs. The stronger intercellular interaction can also lead to an increased flow resistance. For a pair of RBCs with the inclination angle of 0°, when RBCs at upstream of the stenosis are far away from the center of the microvessel, the flow resistance is relatively large. The aggregate formed at the stenosis under a higher intercellular interaction induces a greater flow resistance. The rouleaux formed by a pair of RBCs with the inclination angle of 90° induces larger flow resistance through the stenosis compared to that formed by a pair of RBCs with the inclination angle of 0°.

Although the present study provides a basis for the future investigation on the flow behaviors of multiple interactive RBCs, which compose the real blood, there are some limitations. First, the so-called zero-force distance in the Morse potential is about 13nm [6], which is much smaller than the value we used in the model as it may lead to a high computational cost. Second, only axisymmetric parachute shape and asymmetric slipper are considered for the flow of two RBCs with an initial inclination angle of 90°. The snaking and tumbling RBCs predicted by Fedosov et al. [34] in the cylindrical microchannel as well as the elongated shape in capillary flows [35] are excluded in current study, which occurs at a lower shear rate. Based on the current analysis of two RBCs passing through a microvessel stenosed microvessel, the blood flow consisting of multiple deformable RBCs in a stenosed microvessel would be one of our future studies.

Acknowledgements

Supports given by HKRGC PolyU 5202/13E, PolyU G-YL41, NSFC 51276130, and NIH SC1 CA153325-01 are gratefully acknowledged.

Reference

[1] Bagchi P, Johnson PC, and Popel AS (2005) Computational fluid dynamic simulation of aggregation of deformable cells in a shear flow. J Biomech Eng-T Asme, 2005. 127, 1070-1080.

[2] Rampling MW, et al. (2004) Influence of cell-specific factors on red blood cell aggregation. Biorheology, 2004. 41, 91-112.

[3] Ernst FD (1988) Microcirculation and Hemorheology. Munchen Med Wochen, 1988. 130, 863-866.

[4] Baskurt OK and Meiselman HJ (2007) Hemodynamic effects of red blood cell aggregation. Indian J Exp Biol, 2007. 45, 25-31.

[5] Baumler H, et al. (1999) Basic phenomena of red blood cell rouleaux formation. Biorheology, 1999. 36, 439-442.

[6] Neu B and Meiselman HJ (2002) Depletion-mediated red blood cell aggregation in polymer solutions. Biophys J, 2002. 83, 2482-2490.

[7] Liu YL, et al. (2004) Coupling of Navier-Stokes equations with protein molecular dynamics and its application to hemodynamics. Int J Numer Meth Fl, 2004. 46, 1237-1252.

[8] Lokar M, et al. (2008) Agglutination of like-charged red blood cells induced by binding of beta2-glycoprotein I to outer cell surface. Bioelectrochemistry, 2008. 73, 110-6 doi:10.1016/j.bioelechem.2008.04.015.

[9] Wang T, et al. (2009) Numerical simulation of rheology of red blood cell rouleaux in microchannels. Phys Rev E, 2009. 79.

[10] Li H, Ye T, and Lam KY (2014) Computational Analysis of Dynamic Interaction of Two Red Blood Cells in a Capillary. Cell Biochem Biophys, 2014. 69, 673-680.

[11] Ye T, et al. (2014) Dissipative particle dynamics simulations of deformation and aggregation of healthy and diseased red blood cells in a tube flow. Phys Fluids, 2014. 26.

[12] Shi X, et al. (2013) A lattice Boltzmann fictitious domain method for modeling red blood cell deformation and multiple-cell hydrodynamic interactions in flow. Int J Numer Meth Fl, 2013. 72, 895-911 doi:10.1002/fld.3764.

[13] Smith W, et al. (2004) Retinal arteriolar narrowing is associated with 5-year incident severe hypertension - The Blue Mountains Eye Study. Hypertension, 2004. 44, 442-447 doi:10.1161/01.Hyp.0000140772.40322.Ec.

[14] Vahidkhah K and Fatouraee N (2012) Numerical simulation of red blood cell behavior in a stenosed arteriole using the immersed boundary-lattice Boltzmann method. Int J Numer Meth Bio, 2012. 28, 239-256.

[15] Xu Y-Q, Tian F-B, and Deng Y-L (2013) An Efficient Red Blood Cell Model in the Frame of Ib-Lbm and Its Application. International Journal of Biomathematics, 2013. 06, 1250061 doi:10.1142/s1793524512500611.

[16] Hoogerbrugge PJ and Koelman JMVA (1992) Simulating Microscopic Hydrodynamic Phenomena with Dissipative Particle Dynamics. Europhys Lett, 1992. 19, 155-160.

[17] Espanol P (1995) Hydrodynamics from Dissipative Particle Dynamics. Phys Rev E, 1995. 52, 1734-1742.

[18] Fan XJ, et al. (2006) Simulating flow of DNA suspension using dissipative particle dynamics. Phys Fluids, 2006. 18.

[19] Groot RD and Warren PB (1997) Dissipative particle dynamics: Bridging the gap between atomistic and mesoscopic simulation. J Chem Phys, 1997. 107, 4423-4435.

[20] Fischer TM (2004) Shape memory of human red blood cells. Biophys J, 2004. 86, 3304-3313.
[21] Abkarian M, Faivre M, and Viallat A (2007) Swinging of red blood cells under shear flow. Phys Rev Lett, 2007. 98.
[22] Skotheim JM and Secomb TW (2007) Red blood cells and other nonspherical capsules in shear flow: Oscillatory dynamics and the tank-treading-to-tumbling transition. Phys Rev Lett, 2007. 98.
[23] Li J, et al. (2007) Cytoskeletal dynamics of human erythrocyte. P Natl Acad Sci USA, 2007. 104, 4937-4942.
[24] Pivkin IV and Karniadakis GE (2008) Accurate coarse-grained modeling of red blood cells. Phys Rev Lett, 2008. 101.
[25] Fedosov DA, Caswell B, and Karniadakis GE (2010) A Multiscale Red Blood Cell Model with Accurate Mechanics, Rheology, and Dynamics. Biophys J, 2010. 98, 2215-2225.
[26] Xiao LL, et al. (2016) Numerical simulation of a single cell passing through a narrow slit. Biomech Model Mechanobiol, 2016. doi:10.1007/s10237-016-0789-y.
[27] Fedosov DA, Caswell B, and Karniadakis GE (2010) Systematic coarse-graining of spectrin-level red blood cell models. Comput Method Appl M, 2010. 199, 1937-1948.
[28] Bhattacharjee S, Elimelech M, and Borkovec M (1998) DLVO interaction between colloidal particles: Beyond Derjaguin's approximation. Croat Chem Acta, 1998. 71, 883-903.
[29] Skalak R, Chien S, and Mates RE, *Handbook of bioengineering*. 1987, McGraw-Hill,: New York.
[30] Suresh S, et al. (2005) Connections between single-cell biomechanics and human disease states: gastrointestinal cancer and malaria. Acta Biomater, 2005. 1, 15-30.
[31] Zhang JF, Johnson PC, and Popel AS (2008) Red blood cell aggregation and dissociation in shear flows simulated by lattice Boltzmann method. J Biomech, 2008. 41, 47-55.
[32] Fedosov DA, et al. (2010) Blood Flow and Cell-Free Layer in Microvessels. Microcirculation, 2010. 17, 615-628.
[33] Cokelet GR and Meiselman HJ (1968) Rheological comparison of hemoglobin solutions and erythrocyte suspensions. Science, 1968. 162, 275-7.
[34] Fedosov DA, Peltomaki M, and Gompper G (2014) Deformation and dynamics of red blood cells in flow through cylindrical microchannels. Soft Matter, 2014. 10, 4258-67 doi:10.1039/c4sm00248b.
[35] Noguchi H and Gompper G (2005) Shape transitions of fluid vesicles and red blood cells in capillary flows. P Natl Acad Sci USA, 2005. 102, 14159-14164.